Available online at www.sciencedirect.com
ScienceDirect
Applied Catalysis B: Environmental 80 (2008) 116–121
APPLIED CATALYSIS B: ENVIRONMENTAL
www.elsevier.com/locate/apcatb

# Performance of nano-$Co_3O_4$/peroxymonosulfate system: Kinetics and mechanism study using Acid Orange 7 as a model compound

Xiaoyang Chen [1], Jingwen Chen *, Xianliang Qiao, Degao Wang, Xiyun Cai

*Department of Environmental Science and Technology, Dalian University of Technology, Linggong Road 2, Dalian 116024, PR China*

Received 10 April 2007; received in revised form 13 November 2007; accepted 15 November 2007
Available online 22 November 2007

**Abstract**

Nano-$Co_3O_4$ was prepared by precipitation method and was successfully applied as heterogeneous catalyst to activate peroxymonosulfate (PMS) and degrade a model compound Acid Orange 7 (AO7). The catalyst exhibits spherical morphologies with minor particle agglomeration, small particle average size (20 nm) and high specific surface area (18 $m^2/g$). The degradation kinetics of AO7 induced by nano-$Co_3O_4$/PMS system was investigated at both acidic and neutral pH conditions. The heterogeneous character of PMS activation with nano-$Co_3O_4$ is more pronounced at neutral pH as indicated by fast degradation rate of AO7 and low dissolved Co ion. The catalyst presented a long-term stability through using the catalyst for multiple runs in the degradation of AO7. The main degradation intermediates of AO7 identified by GC/MS and LC/MS were 4-hydroxybenzenesulfonic acid, 1,2-naphthalenedione, coumarin, phthalic anhydride, phthalimide and 2-formyl-benzoic acid. Proposed degradation pathways were elucidated in light of the analyzed degradation products and frontier electron density theory.


*Keywords:* Wastewater treatment; Peroxymonosulfate; Dissolved cobalt ion; Heterogeneous catalysis; Intermediates

## 1. Introduction

Advanced oxidation technologies, which involve in situ generation of highly reactive radicals, such as $^{\bullet}OH$, $^{\bullet}OOH$, $O_2^{\bullet-}$ and $SO_4^{\bullet-}$, have emerged to be promising methods for degradation of organic pollutants [1–3]. In general, $SO_4^{\bullet-}$ that can be produced from scission of peroxide bond by radiolytic, photolytic, thermal activation of persulfate, or electron transfer by transition-metal activation of persulfate or peroxymonosulfate ($KHSO_5$), has powerful oxidizing potential and can degrade many pollutants [4–8]. Among them, cobaltous-mediated decomposition of peroxymonosulfate (Co/PMS) is an efficient catalytic system that can form $SO_4^{\bullet-}$ as major oxidizing species [2,9]. The Co/PMS system for the degradation of contaminants has shown a lot of interests due to their advantages such as high efficiency at wide pH range, small amounts of cobalt catalyst and high efficiency in both carbonate and phosphate buffer solutions [2]. Commercial Oxone ($2KHSO_5{\cdot}KHSO_4{\cdot}K_2SO_4$) can be used to generate PMS, and 614.7 g/L of Oxone is necessary for release of 2 M PMS. For the purpose of practical application, the additional sulfate ions released by Oxone can be reclaimed by ion exchange resin.

Previous studies on Co/PMS system mainly focused on homogeneous catalysis, where cobalt ions has to be separated at the end of the treatment by precipitation due to their toxic nature and thus need additional operational costs [2,7,9]. To avoid the drawback of the homogeneous Co/PMS reagent and broaden the application of the reagent, Dionysiou group investigated heterogeneous activation of PMS with $Co_3O_4$ and found the system had good performance on degradation of 2,4-dichlorophenol [10]. The performance of metal oxides as catalyst mostly depends on the high surface areas and narrow particle size distribution [11]. Nano-materials have attracted great interests in recent years due to their particular physical and chemical properties [11,12]. Hence reducing the diameter of $Co_3O_4$ catalysts to nano-scale may enhance the reactivity. More recently, to increase the catalytic surface area of $Co_3O_4$ particles, Dionysiou group prepared well-dispersed nanocrystalline $Co_3O_4$ particles immobilized on $TiO_2$ support [13,14].

* Corresponding author. Tel.: +86 411 8470 6269; fax: +86 411 8470 6269.
*E-mail addresses:* xiaoyangchen@yahoo.cn (X. Chen), jwchen@dlut.edu.cn (J. Chen).
[1] Current address: Institute of Environmental Resource & Soil Fertilizer, Zhejiang Academy of Agricultural Sciences, Shiqiao Road 198, Hangzhou 310021, PR China.

0926-3373/$ – see front matter © 2007 Elsevier B.V. All rights reserved.
doi:10.1016/j.apcatb.2007.11.009

$TiO_2$ are superior to other supports ($Al_2O_3$ and $SiO_2$) because $TiO_2$ facilitate the formation of surface Co–OH complexes that is considered as the rate-limiting step for PMS activation [14]. Studies about small $Co_3O_4$ particles deposited on other suitable catalytic supports such as Rascing rings and polytetrafluoroethylene were also reported and fast kinetic performance for degradation of contaminants was obtained [15,16].

In this study, nano-$Co_3O_4$ particles were prepared. The performance of nano-$Co_3O_4$/PMS system was investigated using Acid Orange 7 (AO7), a textile azo-dye, as a model compound. Many studies related with AOTs (for example, Fenton, photo-Fenton and $TiO_2$ photocatalysis) used to employ AO7 as models mainly because it is a widely used dye, and resistant to photodegradation and biodegradation [17,18]. To our knowledge, little information on the pathway and mechanism about heterogeneous Co/PMS degradation of AO7 is available from previous studies. Hence this study not only intends to optimize the experimental conditions for AO7 oxidation but also aims to clarify mechanism of AO7 degradation based on intermediate identification and the frontier electron density theory.

## 2. Experimental section

### 2.1. Chemicals

AO7 (98% purity) was supplied by Jierda Dye Chemicals, China. The oxidant Oxone was purchased from Shangyu Jiehua Chemicals, China. $Co(SO_4)_2{\cdot}6H_2O$, $Co(NO_3)_2{\cdot}6H_2O$, $Na_2CO_3$, $NaHCO_3$, *N*-cetyl-*N*,*N*,*N*-trimethyl ammonium bromide (CTAB) and $(CH_3CH_2)_3N$ (TEA) were all analytical grade.

### 2.2. Catalyst preparation and characterization

Nano-$Co_3O_4$ particles were prepared as described by Zhou et al. [12], and characterized by X-ray diffraction (XRD) using a diffractometer with Cu Ka radiation (Shimadzu LabXXRD-6000). The microstructure was examined by transmission electron microscopy (TEM, JEM-2000EX) at accelerating voltage of 200 kV. The Brunauer–Emmett–Teller (BET) specific surface area of the catalyst was measured by nitrogen adsorption at 77 K using a Quantachrome NOWA 4000 apparatus.

### 2.3. Heterogeneous $Co_3O_4$/PMS reactions

The degradation experiments were conducted in a 500 mL vessel. At given reaction time intervals, samples were taken for analysis. For the UV–vis measurement, methanol with the same volume as the samples was used to quench the reaction. Since PMS is an acidic oxidant, the addition of PMS led to a significant decrease of pH, the experiment was conducted both at acidic (pH 2–3, no adjustment) and neutral (pH 7.0, adjusted with 0.5 M bicarbonate solution) conditions. For the TOC analysis, phosphate buffer solution (0.05 M) instead of bicarbonate was used to maintain the neutral condition (pH 7.0) of the solution and sodium nitrite was used as quenching reagent instead. Most of the experiments were conducted in triplicate. During the recycling experiment of the catalyst, the catalyst was separated and thoroughly washed with distilled water and ethanol after each recycle. Then the catalyst was dried at 120 °C for 8 h to remove water and ethanol.

### 2.4. Analytical methods

AO7 concentration was measured by a UV–vis spectrophotometer (Hitachi U2800) at wavelength of 486 nm. Prior to the measurement, a calibration curve (from 0 to 0.1 mM AO7) was obtained using standard AO7 solutions. A Shimazu TOC-$V_{CPH}$ analyzer was employed for TOC measurement. To monitor Co leaching from the nano-$Co_3O_4$ catalyst, samples were filtered with 0.22 μm filters, and analyzed with graphite furnace atomic absorption spectrophotometer (PerkinElmer AA-700).

For GC/MS analysis, the samples (20 mL) were quenched by 10 mL of $NaNO_2$ solution (40 g/L) and acidified (pH < 2). After adding NaCl solid quantitatively, the samples were extracted with dichloromethane (3× 30 mL). The extracts were dried on anhydrous sodium sulfate and then concentrated to 1 mL. GC/MS analyses were performed on an Agilent GC/6890N coupled with MSD/5975. EI mode was adopted. The analytical column was an HP-5MS capillary column (30 m × 0.32 mm × 0.25 μm). The GC column was operated in a temperature programmed mode with an initial temperature of 40 °C held for 2 min, ramped first at 100 °C with a 12 °C/min rate, then to 200 °C with 5 °C/min and finally ramped to 270 °C with a 20 °C/min rate, and held at 270 °C for 10 min. Injection volume was 1 μL with 1.0 mL/min helium as a carrier gas. Identification of the GC/MS spectral features was achieved with the use of a built-in library. All library-matched species exhibited the degree of match better than 90%.

For LC/MS analysis, the samples were directly injected into the instrument without pre-preparation. An Agilent-1100 series LC-MSD-Trap (G2445A) with a Hypersil-ODS $C_{18}$ inverse phase column (4.6 mm × 250 mm, i.d. 5 μm) was used, and ESI mode was adopted. Gradient elution was made up using binary gradient of acetonitrile (A) and ammonium acetate 10 mM (B) as follows: 2% of A in 5 min at flow rate 0.5 mL/min, and 2% of A in 7 min at flow rate 1.2 mL/min, and then linear gradient from 2% to 95% of A in 30 min at flow rate 1.2 mL/min. Full-scan spectra were recorded from *m*/*z* 100–500. The instrument was operated in both positive and negative ion mode.

### 2.5. Quantum chemical computation

According to the frontier molecular orbital theory, for a radical reaction, the point of attack is at the position where the highest density of the sum of each electron occurs when they are in the highest occupied molecular orbital (HOMO) and lowest unoccupied molecular orbital (LUMO), respectively [19–21]. The frontier electron density $f_r$ can be calculated as

$$f_r = \sum\nolimits_i \left(C_{ri}^{\mathrm{HOMO}}\right)^2 + \sum\nolimits_i \left(C_{ri}^{\mathrm{LUMO}}\right)^2 \quad (1)$$

where $C_{ri}^{\mathrm{HOMO}}$ and $C_{ri}^{\mathrm{LUMO}}$ are the coefficients of the atomic orbital in the HOMO and LUMO, respectively, and $r$ is the

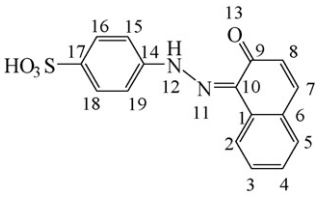

Fig. 1. Molecular structure of AO7.

number of atoms orbitals. The highest $f_r$ value indicates the most reactive position that most likely to be attacked by a radical.

All the quantum chemical calculations were performed with Gaussian-03 program. The calculated geometries of AO7 (hydrazone form, Fig. 1) were fully optimized using hybrid density functional B3LYP with the STO-3G basis set. The highest occupied molecular orbital (HOMO) and lowest unoccupied molecular orbital (LUMO) electron densities for every atoms of AO7 were calculated on the base of the fully optimized geometries of AO7.

## 3. Results and discussion

### 3.1. Catalyst characterization

As shown by Fig. 2, XRD patterns demonstrate the cubic structure of the prepared $Co_3O_4$. The particle size estimated from the (3 1 1) plane using the Debye–Scherrer equation was 18 nm. The BET specific surface area of the prepared catalyst was 18 $m^2/g$.

The microstructure of the prepared catalyst powder is presented in Fig. 3, which reveals that the particles exhibit spherical morphologies with minor particle agglomeration and a relatively narrow particle size distribution. The average particle diameter of catalyst is about 20 nm, which is consistent with the XRD analysis.

### 3.2. Catalytic activity of nano-$Co_3O_4$

The degradation kinetics of AO7 under different reaction conditions is shown in Fig. 4. In the presence of 2 mM PMS only, and without nano-$Co_3O_4$ and pH adjustment, no

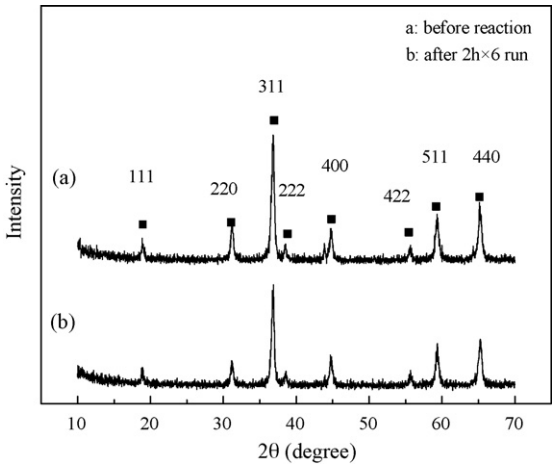


Fig. 2. XRD patterns of nano-$Co_3O_4$ catalyst.

degradation of AO7 can be observed (curve a). With nano-$Co_3O_4$ only and without PMS, nearly 12% of AO7 was removed in the first 60 min probably due to the adsorption of AO7 on the surface of the catalyst (curve b). At neutral pH adjusted by bicarbonate, with 2 mM PMS and without nano-$Co_3O_4$, about 12% of AO7 degraded in the first 60 min due to possible generation of percarbonate from the interaction of bicarbonate species and PMS. With the nano-$Co_3O_4$/PMS system, the oxidation of AO7 is quite significant both at acidic and neutral pH, where the oxidation of AO7 by the reactive radicals from Co/PMS system is the main process (curves d and e).

Which is the main process, heterogeneous nano-$Co_3O_4$/PMS or homogeneous Co/PMS degradation of AO7? To clarify the mechanism, the concentration of dissolved Co ions leached from the nano-$Co_3O_4$ catalyst was measured and the results are presented in Fig. 5. It is shown that under acidic condition, Co dissolved slowly from nano-$Co_3O_4$, reaching a value of 0.61 mg/L after 2 h of reaction. Thus, nano-$Co_3O_4$ was not stable under acidic condition. While at neutral condition, dissolved Co was always below 0.05 mg/L, thus very limited cobalt dissolved from nano-$Co_3O_4$. The result is consistent with the results of Dionysiou group [10].

To evaluate the contribution of dissolved Co to the degradation of AO7, homogeneous experiments with $Co^{2+}$ concentration that equals to the leached from nano-$Co_3O_4$ were

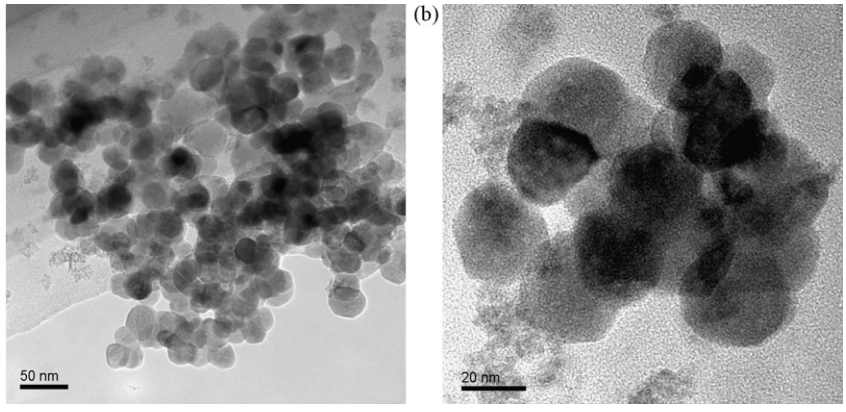


Fig. 3. TEM photographs of nano-$Co_3O_4$ catalyst.

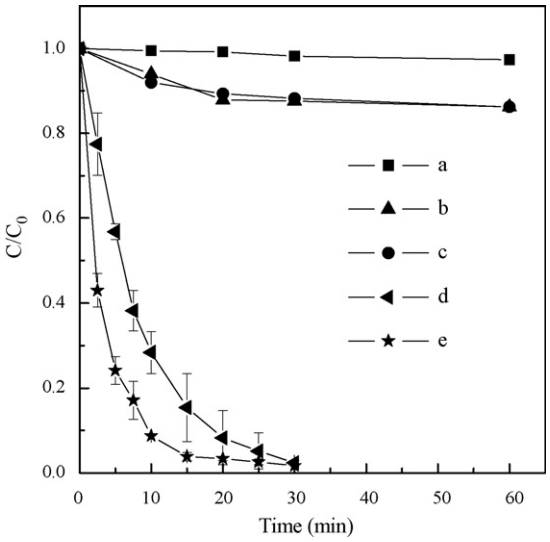


Fig. 4. Degradation kinetics of 0.2 mM AO7 under different conditions: (a) 2 mM PMS, (b) 0.5 g/L nano-$Co_3O_4$, (c) 2 mM PMS (neutral pH), (d) 0.5 g/L nano-$Co_3O_4$ + 2 mM PMS (acidic pH) and (e) 0.5 g/L nano-$Co_3O_4$ + 2 mM PMS (neutral pH).

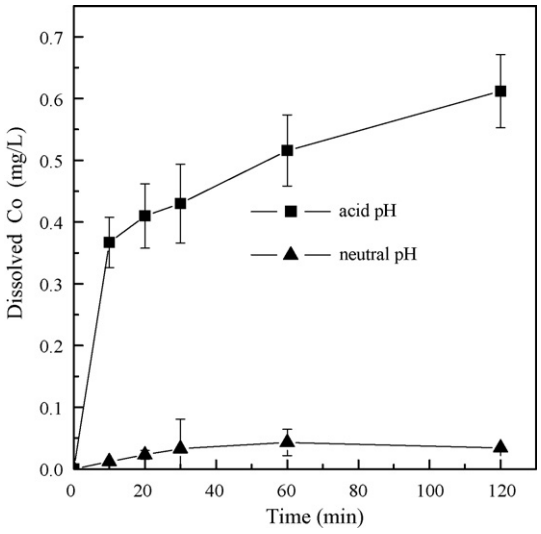


Fig. 5. Dissolution of Co from nano-$Co_3O_4$ under acidic and neutral pH. Conditions: $[AO7]_0$ = 0.2 mM, [nano-$Co_3O_4$] = 0.5 g/L and [PMS] = 2 mM.

conducted. As can be observed from Fig. 6, the initial degradation rate of AO7 was much faster when nano-$Co_3O_4$ was added. Thus the main catalytic contribution is from nano-$Co_3O_4$, not dissolved Co ions, whether at acidic or neutral pH. The heterogeneous catalysis of nano-$Co_3O_4$ was especially prominent under neutral pH, since the homogeneous catalysis was limited owing to low concentration of dissolved Co ions. Most dyestuff wastewaters are neutral since they usually contain large amount of buffer salts. Thus the nano-$Co_3O_4$/PMS system is quite acceptable from application point of view due to its very low dissolution of Co ions and high reactivity.

### 3.3. Effects of PMS dosage on the degradation of AO7

The effect of PMS versus AO7 molar ratio ([PMS]/[AO7]) on the mineralization degree of AO7 was investigated in phosphate buffer (0.05 M), and the results are depicted in Fig. 7. The mineralization degree increases with increasing the molar ratio when [PMS]/[AO7] < 60. When [PMS]/[AO7] > 60, a constant mineralization degree (70%) was reached, thus TOC could not be totally removed due to the barrier of mineralization. When PMS alone ([PMS]/[AO7] = 60) was used in phosphate buffer (0.05 M), limited TOC (8%) was removed due to the interaction of PMS with phosphate species, which is similar to the observations of Dionysiou group who found limited 2,4-dichlorophenol transformation when PMS alone was used in buffered water due to the interaction with bicarbonate species and probably the generation of percarbonate [10]. The presence of phosphate and carbonate species usually leads to a decrease of reactivity in other hydroxyl radical-based AOTs such as Fenton and $TiO_2$ photocatalysis system [22,23]. From this point of view, Co/PMS is superior to other hydroxyl radical-based AOTs especially in the presence of phosphate and carbonate species.

### 3.4. Stability of nano-$Co_3O_4$ catalyst in multiple runs

Six recycling runs of the nano-$Co_3O_4$ catalyst were carried out. As shown in Fig. 8, the regenerated catalyst exhibits good performance and stability. The degradation rate of AO7

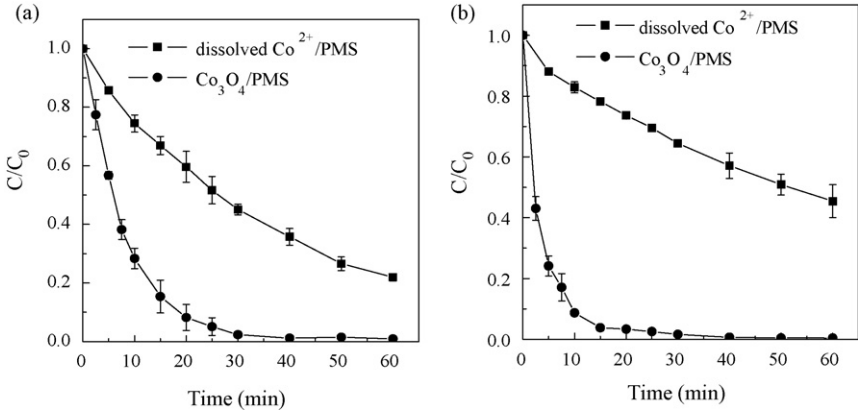


Fig. 6. Degradation of AO7 with heterogeneous nano-$Co_3O_4$/PMS and homogeneous $Co^{2+}$/PMS at (a) acidic condition ($[Co^{2+}]$ = 0.61 mg/L) and (b) neutral condition ($[Co^{2+}]$ = 0.05 mg/L). Conditions: $[AO7]_0$ = 0.2 mM, [PMS] = 2 mM and [nano-$Co_3O_4$] = 0.5 g/L.

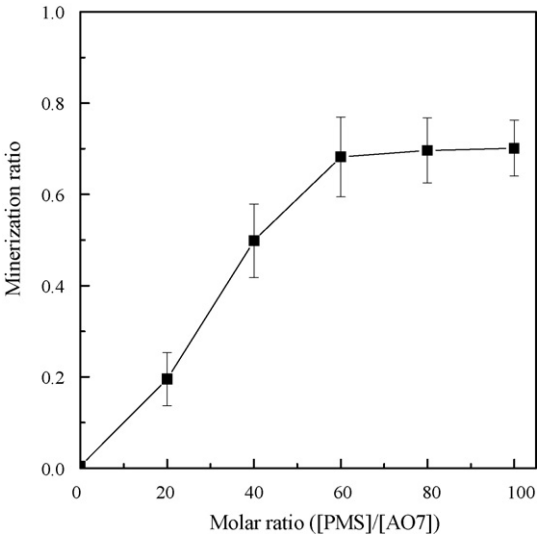


Fig. 7. Effect of PMS dosage on the mineralization of AO7. $[AO7]_0 = 0.2$ mM, [nano-$Co_3O_4$] = 0.5 g/L, 0.05 M phosphate buffer (pH 7.0).

remained almost unchanged compared to the fresh catalyst. The concentration of dissolved Co ions from $Co_3O_4$ was almost the same as the fresh catalyst (results not shown). To further investigate the stability of the nano-$Co_3O_4$ catalyst, the catalyst after six cycles was examined by XRD and the pattern is shown in Fig. 2 (curve b). There are little differences between the two patterns (curves a and b), indicating no obvious change in $Co_3O_4$ crystallite during the reaction. Good catalytic performance and little ion leaching indicates that the catalyst has an excellent long-term stability, which could be attributed to the stable structure of the nano-$Co_3O_4$ catalyst.

### 3.5. Degradation pathway of AO7

Five main intermediates, 1,2-naphthoquinone, coumarin, phthalic anhydride, phthalimide and 2-formyl-benzoic acid were detected by GC/MS. The molecular ion and spectrometric fragmentation peaks for the five products are given in Figures S1–S5. Two main intermediates, 4-hydroxybenzenesulfonic acid and 1,2-naphthoquinone were detected by LC/MS and the

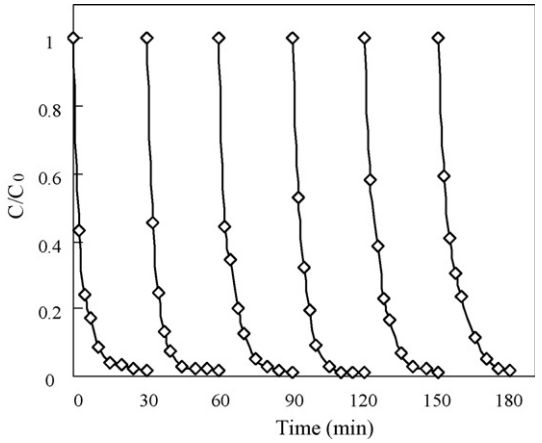


Fig. 8. Cyclic degradation of AO7 as a function of time in the presence of PMS at neutral pH. $[AO7]_0 = 0.2$ mM, [nano-$Co_3O_4$] = 0.5 g/L and [PMS] = 2 mM.

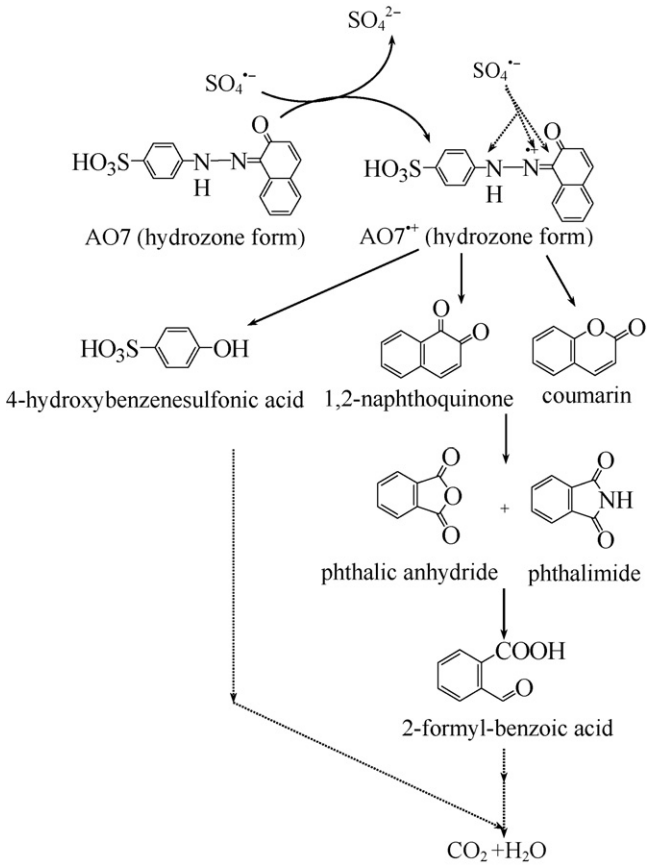


Fig. 9. Possible pathways of AO7 oxidative degradation with nano-$Co_3O_4$/PMS system.

fragmentation pattern are shown in Figures S6 and S7. Totally, six main intermediates were detected.

To know the position of AO7 that is most likely to be attacked by a radical, $f_r$ of individual atoms of AO7 molecule were calculated using Gaussian-03 program in conjunction with Eq. (1), and atom numbers corresponds to Fig. 1. Here the calculated molecule is hydrazone form of AO7, the predominant species in the current study due to intermolecular proton transfer of azo form [24]. The $f_r$ values for N11 and N12 atoms are the highest, thus $SO_4^{\bullet-}$ most preferentially attack these positions. The products of 1,2-naphthoquinone and 4-hydroxybenzenesulfonic acid confirm that $SO_4^{\bullet-}$ firstly attack at N11 and N12, which can produce phenyl and naphthalene intermediates. The calculated results also show that $f_r$ of C10 is the highest among all the C atoms, hence C10 becomes another possible attacking point, and the intermediate coumarin supports the pathway. Though $f_r$ of O13 is also high, it is not the active position due to the high oxidative state. Thus the theoretical analysis is consistent with the experimental results.

Coumarin and 1,2-naphthoquinone can be further degraded to phthalic anhydride and phthalimide. $SO_4^{\bullet-}$ is a very strong one-electron oxidant with redox potential estimated to be 2.5–3.1 V versus normal hydrogen electrode [25]. Hence $NO_3^{\bullet-}$ can be formed through the reaction of $SO_4^{\bullet-}$ and $NO_3^-$, and phthalimide becomes the products in the oxidation reaction process involving $NO_3^{\bullet-}$. Phthalic derivatives, such as phthalic

anhydride and phthalimide were also observed with low concentrations in photocatalytic degradation of AO7 reactions [18,26]. Stylidi et al. [18,26] deduced that the phthalic derivatives were the further degradation products of intermediates with naphthalene ring, such as 1,2-naphoquinone and coumarin. Dionysiou group also observed that the major intermediates for $SO_4^{\bullet-}$ attack on phenol were similar to the $^{\bullet}OH$ involving oxidations such as Fenton reagent, sonolysis, ozonolysis and photocatalysis [27].

According to the theoretical analysis and the identified intermediates, the possible pathway of AO7 oxidative degradation with nano-$Co_3O_4$/PMS system is proposed, as shown in Fig. 9. First, $SO_4^{\bullet-}$ most probably attacks on N11 of AO7, leading to the formation of $AO7^{\bullet+}$ via electron transfer from the compound to $SO_4^{\bullet-}$ [10,27,28]. Then $SO_4^{\bullet-}$ further reacts with $AO7^{\bullet+}$, and attacks on the N–N and C=N where the naphthalene ring and phenyl ring link up. AO7 may be decomposed to phenyl intermediates (4-hydroxybenzenesulfonic acid), and naphthalene intermediates (1,2-naphthalenedione and coumarin). Then these intermediates are oxidized to phthalic anhydride and phthalimide, and further oxidized to ring opening products 2-formyl-benzoic acid, finally mineralized to $CO_2$, $H_2O$ and inorganic ions.

## 4. Conclusions

Nano-$Co_3O_4$ with small particle size and high specific surface area was prepared by precipitation method. The catalyst exhibits good heterogeneous activity in nano-$Co_3O_4$/PMS system and low dissolved Co ions especially at neutral conditions. The catalyst has an excellent long-term stability. Possible degradation pathway of AO7 induced by heterogeneous nano-$Co_3O_4$/PMS system is proposed by theoretical analysis and degradation products determination. The results indicated that the key step of AO7 degradation was the cleavage of N–N and C=N bonds where phenyl ring and naphthalene ring link up.

## Acknowledgements

Prof. Ce Hao is greatly acknowledged for assisting the Gaussian-03 calculations. The study was supported by the National Basic Research Program of China (Project 2003CB415006), National Natural Science Foundation (No. 20337020) of China, and the ''Key Laboratory of Industrial Ecology and Environmental Engineering, MOE''. Computational resources used in this study were provided by Shenteng 1800 High Performance Computing Center.

## Appendix A. Supplementary data

Supplementary data associated with this article can be found, in the online version, at doi:10.1016/j.apcatb.2007.11.009.

## References

[1] E. Chamarro, A. Marco, S. Esplugas, Water Res. 35 (2001) 1047.
[2] G.P. Anipsitakis, D.D. Dionysiou, Environ. Sci. Technol. 37 (2003) 4790.
[3] M. Cheng, W. Ma, J. Li, Y. Huang, J.C. Zhao, Y.X. Wen, Y. Xu, Environ. Sci. Technol. 38 (2004) 1569.
[4] M.-S. Tsao, W.K. Wilmarth, J. Phys. Chem. 63 (1959) 346.
[5] P. Neta, V. Madhavan, H. Zemel, R.W. Fessenden, J. Am. Chem. Soc. 99 (1977) 163.
[6] C.J. Liang, C.J. Bruell, M.C. Marley, K.L. Sperry, Soil Sediment Contam. 12 (2003) 207.
[7] G.P. Anipsitakis, D.D. Dionysiou, Environ. Sci. Technol. 38 (2004) 3705.
[8] H. Hori, A. Yamamoto, E. Hayakawa, S. Taniyasu, N. Yamashita, S. Kutsuna, H. Kiatagawa, R. Arakawa, Environ. Sci. Technol. 39 (2005) 2383.
[9] J. Fernandez, P. Maruthamuthu, A. Renken, J. Kiwi, Appl. Catal. B: Environ. 49 (2004) 207.
[10] G.P. Anipsitakis, E. Stathatos, D.D. Dionysiou, J. Phys. Chem. B. 109 (2005) 13052.
[11] Y. Jiang, Y. Wu, B. Xie, Y. Xie, Y. Qian, Mater. Chem. Phys. 74 (2002) 234.
[12] L. Zhou, J. Xu, H. Miao, F. Wang, X. Li, Appl. Catal. A: Gen. 292 (2005) 223.
[13] Q. Yang, H. Choi, D.D. Dionysiou, Appl. Catal. B: Environ. 74 (2007) 170.
[14] Q. Yang, H. Choi, Y. Chen, D.D. Dionysiou, Appl. Catal. B: Environ. 77 (2007) 300.
[15] Z. Yu, M. Bensimon, D. Laub, L. Kiwi-Minsker, W. Jardim, E. Mielczarski, J. Mielczarski, J. Kiwi, J. Mol. Catal. A: Chem. 272 (2007) 11.
[16] P. Raja, M. Bensimon, U. Klehm, P. Albers, D. Laub, L. Kiwi-Minsker, A. Renken, J. Kiwi, J. Photochem. Photobiol. A 187 (2007) 332.
[17] C.W. Scheeren, J.N.G. Paniz, A.F. Martins, J. Environ. Sci. Heal. A 37 (2002) 1253.
[18] M. Stylidi, D.I. Kondarides, X.E. Verykios, Appl. Catal. B: Environ. 47 (2004) 189.
[19] G. Liu, X. Li, J. Zhao, S. Horikoshi, H. Hidaka, J. Mol. Catal. A: Chem. 153 (2000) 221.
[20] B.-D. Lee, M. Iso, M. Hosomi, Chemosphere 42 (2001) 431.
[21] N. San, A. Hatipoğlu, G. Koçtűrk, Z. Çinar, J. Photochem. Photobiol. A: Chem. 146 (2002) 189.
[22] J. Kochany, E. Lipczynska-Kochany, Chemosphere 25 (1992) 1769.
[23] B. Neppolian, H.C. Choi, S. Sakthivel, B. Arabindoo, V. Murugesan, Chemosphere 46 (2002) 1173.
[24] T. Hihara, Y. Okada, Z. Morita, Dyes Pigments 59 (2003) 201.
[25] P. Neta, R.E. Huie, A.B. Ross, J. Phys. Chem. Ref. Data 17 (1988) 1027.
[26] M. Stylidi, D.I. Kondarides, X.E. Verykios, Appl. Catal. B: Environ. 40 (2003) 271.
[27] G.P. Anipsitakis, D.D. Dionysiou, M.A. Gonzalez, Environ. Sci. Technol. 40 (2006) 1000.
[28] S. Das, P.V. Kamat, S. Padmaja, V. Au, S.A. Madison, J. Chem. Soc., Perkin Trans. 2 (1999) 1219.